Predictive In Vitro-In Vivo Extrapolation for Time Dependent Inhibition of CYP1A2, CYP2C8, CYP2C9, CYP2C19, and CYP2D6 Using Pooled Human Hepatocytes, Human Liver Microsomes, and a Simple Mechanistic Static Model[S]

Diane Ramsden,[1] Elke S. Perloff,[1] Andrea Whitcher-Johnstone, Thuy Ho, Reena Patel, Kirk D. Kozminski, Cody L. Fullenwider, and J. George Zhang

Takeda Development Center Americas, Inc., Cambridge, Massachusetts (D.R.); Corning Gentest Contract Research Services, Corning Life Sciences, Woburn, Massachusetts (E.S.P., T.H., R.P., J.G.Z.); Takeda Development Center Americas, Inc., San Diego, California (K.D.K., C.L.F.); and Boehringer Ingelheim Pharmaceuticals Inc., Ridgefield, Connecticut (A.W.-J.)

ABSTRACT

Inactivation of Cytochrome P450 (CYP450) enzymes can lead to significant increases in exposure of comedicants. The majority of reported in vitro to in vivo extrapolation (IVIVE) data have historically focused on CYP3A, leaving the assessment of other CYP isoforms insubstantial. To this end, the utility of human hepatocytes (HHEP) and human liver microsomes (HLM) to predict clinically relevant drug-drug interactions was investigated with a focus on CYP1A2, CYP2C8, CYP2C9, CYP2C19, and CYP2D6. Evaluation of IVIVE for CYP2B6 was limited to only weak inhibition. A search of the University of Washington Drug-Drug Interaction Database was conducted to identify a clinically relevant weak, moderate, and strong inhibitor for selective substrates of CYP1A2, CYP2C8, CYP2C9, CYP2C19, and CYP2D6, resulting in 18 inhibitors for in vitro characterization against 119 clinical interaction studies. Pooled human hepatocytes and HLM were preincubated with increasing concentrations of inhibitors for designated timepoints. Time dependent inhibition was detected in HLM for four moderate/strong inhibitors, suggesting that some optimization of incubation conditions (i.e., lower protein concentrations) is needed to capture weak inhibition. Clinical risk assessment was conducted by incorporating the in vitro derived kinetic parameters maximal rate of enzyme inactivation (min^{-1}) (k$_{inact}$) and concentration of inhibitor resulting in 50% of the maximum enzyme inactivation (K$_I$) into static equations recommended by regulatory authorities. Significant overprediction was observed when applying the basic models recommended by regulatory agencies. Mechanistic static models, which consider the fraction of metabolism through the impacted enzyme, using the unbound hepatic inlet concentration lead to the best overall prediction accuracy with 92% and 85% of data from HHEPs and HLM, respectively, within twofold of the observed value.

SIGNIFICANCE STATEMENT

Coupling time-dependent inactivation parameters derived from pooled human hepatocytes and human liver microsomes (HLM) with a mechanistic static model provides an easy and quantitatively accurate means to determine clinical drug-drug interaction risk from in vitro data. Optimization is needed to evaluate time-dependent inhibition (TDI) for weak and moderate inhibitors using HLM. Recommendations are made with respect to input parameters for in vitro to in vivo extrapolation (IVIVE) of TDI with non-CYP3A enzymes using available data from HLM and human hepatocytes.

Introduction

Evaluating the potential for a drug candidate to inactivate Cytochrome P (CYP450) enzymes is important to predict the likelihood of clinically relevant drug-drug interactions (DDIs). Enzyme inactivation is a process whereby, during the catalytic cycle of an enzyme, a reactive intermediate is produced that binds to and irreversibly inhibits the active site of that enzyme. Competitive inhibition and inactivation are mechanistically distinct processes: in the case of competitive inhibition,

ABBREVIATIONS: C$_{max,ss}$, maximal observed concentration in blood at steady state; C$_{max,ss,u}$, maximal unbound plasma concentration at steady state; CYP, cytochrome P450; DDI, drug-drug interaction; EMA, European Medicines Agency; FDA, Food and Drug Administration; F$_m$, fraction metabolized through the pathway; FN, false negatives; GMFE, geometric mean fold error; HHEP, human hepatocytes; HLM, human liver microsomes; I$_{inlet,max,u}$, unbound hepatic inlet concentration; IVIVE, in vitro to in vivo extrapolation; K$_i$, inhibition constant for reversible inhibition; k$_{inact}$, maximal rate of enzyme inactivation (min^{-1}); K$_I$, concentration of inhibitor resulting in 50% of the maximum enzyme inactivation; k$_{obs}$, first order rate constant for inactivation estimated from the slope of residual activity (ln) versus preincubation time at each inhibitor concentration (min^{-1}); k$_{solvent}$, first order rate constant for inactivation estimated from the slope of residual activity (ln) versus preincubation time for the solvent control [min^{-1}] (may be constrained to equal the k$_{obs}$ for the vehicle control); LC-MS/MS, liquid chromatography tandem mass spectrometry; ln, natural log residual activity; MM, Michaelis-Menten; MSM, mechanistic static model; PBPK, Physiologically-Based Pharmacokinetic; RMSE, root mean square error; PMDA, Pharmaceutical and Medical Devices Agency; TDI, time-dependent inhibition; UW-DIDB, University of Washington Drug-Drug Interaction Database; WME, William's medium E.

enzyme activity is restored when the inhibitor is removed, whereas removal of the inactivator does not restore the activity of the inactivated enzyme. Consequently, recovery of enzyme activity depends on the rate of enzyme resynthesis. Regulatory agencies have provided industry guidance on the conduct of in vitro studies to predict the potential of a drug to mediate DDI through enzyme inactivation [European Medicines Agency (EMA), Food and Drug Administration (FDA) and Pharmaceutical and Medical Devices Agency (PMDA)]. Currently, human liver microsomes (HLM) or recombinantly expressed enzymes are the in vitro systems most often used to evaluate CYP450 inactivation (Grimm et al., 2009); however, although HLM have been successfully used to predict clinically relevant DDIs for known CYP450 inactivators (Obach et al., 2007), there is a tendency to overpredict clinical DDIs (Chen et al., 2011). As with any in vitro system, the environment of the typical microsomal and recombinant enzyme assays differs significantly from the in vivo environment that they strive to model. Consequently, assumptions are made about a drug, for example, complete permeability across biologic membranes, minimal binding to microsomal proteins, and minimal contribution of non-CYP450 metabolism. By using a more physiologically complete system such as human hepatocytes, which have an intact plasma membrane, functional membrane transporters, a complete set of hepatic CYP450 and non-CYP450 enzymes, some assumptions associated with HLM and recombinant systems may no longer be necessary. Although human hepatocytes can be used to evaluate the potential for CYP450 inactivation, there are only a few peer-reviewed examples, prompting the need for additional research as a prerequisite for more routine use of this model. Nevertheless, human hepatocytes could provide mechanistic insight that supports conventional inactivation studies where non-CYP450 metabolites are generated or significant intracellular accumulation of a drug is suspected. In human hepatocytes, active transport of a drug into or out of cells can affect the concentration of a drug present at the CYP450 active site, ultimately affecting the inactivation parameters determined. Xu et al. and Chen et al. postulated that differences in inactivation parameters between human hepatocytes and HLM were due to active transport of drugs in hepatocytes (Xu et al., 2009; Chen et al., 2011). A decrease in active uptake of a compound with limited permeability will decrease the inactivation potential by decreasing the concentration of a drug at the site of inactivation. Conversely, a decrease in active efflux will increase the inactivation potential by increasing the amount of a drug available for metabolism (Lam et al., 2006). Indeed, erythromycin, diltiazem, and troleandomycin are known or suspected substrates of membrane transporters and result in the greatest discrepancy in inactivation parameters between HLM and hepatocytes (Seelig and Landwojtowicz, 2000; Kostrubsky et al., 2003; Kurnik et al., 2006). Additionally, CYP450 inactivators subject to extensive non-CYP450 metabolism, for example, glucuronidation in vivo, may be mistakenly determined to be clinically relevant inactivators when evaluated using HLM. For example, ezetimibe, a cholesterol-lowering drug, displayed potent in vitro inactivation of CYP3A4 using HLM but did not result in clinically meaningful inhibition, likely due to its extensive glucuronidation (Parkinson et al., 2010). Alternatively, a drug that is significantly metabolized via a non-CYP450 pathway and forms a metabolite that inactivates CYP450 enzymes cannot be detected in conventional microsomal CYP450 inactivation assays, as was observed with an aldehyde oxidase metabolite (Zetterberg et al., 2016). This was also the case with gemfibrozil, which led to significant CYP2C8 DDIs subsequently revealed to be mediated by its major metabolite gemfibrozil-1-O-β-glucuronide, the potential for DDIs could have been detected if the inactivation studies were initially performed using human hepatocytes (Ogilvie et al., 2006; Parkinson et al., 2010). Although IVIVE efforts for time-dependent inhibition (TDI) have focused primarily on CYP3A inactivation (Eng et al., 2020), it is unclear whether the recommendations made for CYP3A inactivators may translate to other major CYPs or whether hepatocytes could also be a predictive in vitro model to assess TDI of other CYP isoforms. The purpose of the work described here was to assess suspended hepatocytes and HLM as tools for predicting DDI caused by TDI of CYPs 1A2, 2C8, 2C9, 2C19, and 2D6.

Materials and Methods

Chemicals and Reagents

Cryopreserved Hepatocyte Recovery Medium was purchased from Life Technology (cat # CM7000, Carlsbad, CA). Pooled 200 donor mixed gender human liver microsomes were purchased from XenoTech (cat# H2610, Kansas City, KS). Cimetidine, ciprofloxacin, clopidogrel, dronedarone, fluconazole, fluvoxamine,
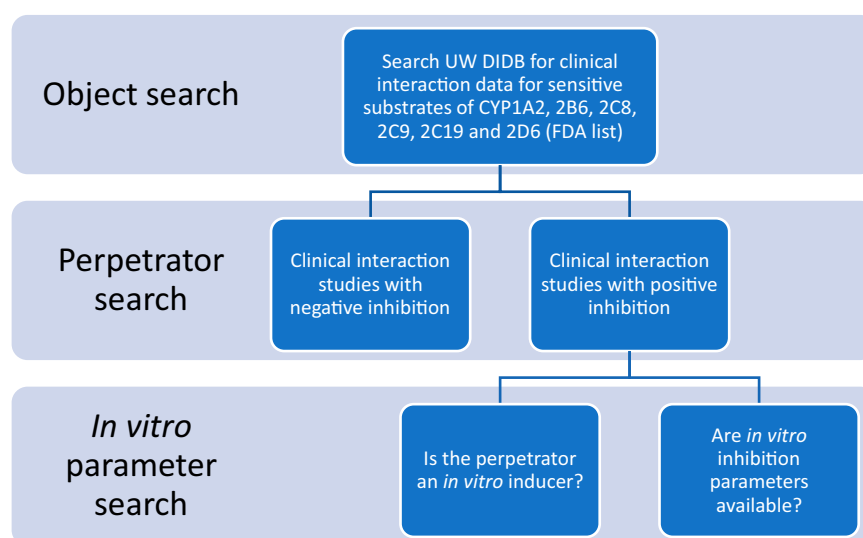
Fig. 1. The workflow for identifying clinically relevant inhibitors included searching the UW-DIDB for clinical data with sensitive objects of CYPs 1A2, 2B6, 2C8, 2C9, 2C19, and 2D6. The data were collated for both positive and negative inhibition, and perpetrators were categorized as negative, weak, moderate, or strong inhibitors dependent on the magnitude of AUC change. Where negative inhibition was defined as AUCR between 1.0- and 1.25-fold, weak was between 1.25- and 2.0-fold AUCR, moderate between 2.0- and 5.0-fold AUCR and strong >5.0-fold AUCR. Once perpetrators were identified, literature searches were performed for existing in vitro data, including inhibition and time-dependent inhibition, induction and transporter substrate, or inhibition observations.

TABLE 1

Enzyme reaction conditions

CYP Isoform	P450 Probe Substrate		Substrate Concentration (μM)		Incubation Time (min)	
	HHEP	HLM	HHEP	HLM	HHEP	HLM
CYP1A2	Phenacetin	Phenacetin	100	180	30	8
CYP2C8	Amodiaquine	Paclitaxel	100	40	10	12
CYP2C9	Diclofenac	Diclofenac	100	36	10	8
CYP2C19	s-Mephenytoin	s-Mephenytoin	100	225	30	8
CYP2D6	Dextromethorphan	Dextromethorphan	25	36	10	8

HLM final protein concentration (1 mg/mL).

miconazole, moclobemide, omeprazole, paroxetine, tasisulam, ticlopidine trimetho-prim, NADPH, and William's medium E were purchased from Millipore Sigma (St. Louis, MO). Mirabegron was obtained from MyBioSource (San Diego, CA), osilodrostat from Selleck Chemicals (Houston, TX), and gemfibrozil from Toronto Research Chemicals (Toronto, ON).

Hepatocytes

Experiments were performed using cryopreserved human hepatocytes (Cat. # 454427, Corning Life Sciences, Woburn, MA) pooled from three donors (lot # 305, 346, and 347, except for ticlopidine, which used lot #305, 289, and 293). Donor demographics are displayed in Supplemental Table 1.

Methods

Identification of Clinically Relevant Inhibitors for IVIVE Analysis. Clinical data were collected according to Fig. 1, by searching the University of Washington Drug-Drug Interaction Database (UW-DIDB) for published studies with and without observed changes in area under the curve (AUC) or clearance for sensitive substrates of CYP1A2, CYP2B6, CYP2C8, CYP2C9, CYP2C19, and CYP2D6, indicated on the FDA website (https://www.fda.gov/drugs/drug-interactions-labeling/drug-development-and-drug-interactions-table-substrates-inhibitors-and-inducers), Supplemental Table 2. Clinical data were reviewed to select for multiple dose studies and to identify weak, moderate, and strong inhibitors toward each enzyme. Inhibitors with multiple studies against multiple substrate drugs were prioritized to expand the dataset available for IVIVE analysis and evaluate trends across selective substrates (Table 4). Once clinically relevant inhibitors were identified, the UW-DIDB was searched for in vitro inhibition and induction parameters and for transporter substrate and inhibitor liabilities. Additionally, inhibitor properties including dose level used, maximal observed concentration in blood at steady state ($C_{max,ss}$), Fu, Ka, Fa, Fg Rb, and LogP or D were collected where possible. The $C_{max,ss}$

values, published solubility, and historical in vitro inhibition data were used to identify relevant in vitro test concentrations with the goal being to span concentrations that would enable estimation of the kinetic parameters but limit the likelihood to observe toxicity.

Compilation of In Vitro Parameters from Literature. To expand the analysis to understand whether the recommendations identified for improving the prediction of TDI for CYPs 1A2, 2C8, 2C9, 2C19, and 2D6 could be extended to data generated in HLM, an attempt was made to collate time-dependent inhibition parameters from literature. This was accomplished by searching the UW-DIDB for inhibition parameters derived from either human hepatocytes or HLM and analysis was extended to CYP2B6. Data compiled from literature are presented in Supplemental Table 7. Additionally, HLM incubations were conducted within Takeda, using standard experimental conditions for inhibitors with no published data.

Experimental. *Hepatocyte incubations.* Hepatocytes from three individual lots (reference Supplemental Table 1) were thawed and pooled in Cryopreserved Hepatocyte Recovery Medium, then centrifuged at 100 g for 10 minutes at room temperature. The supernatant was aspirated, and the pellet was washed with William's medium E (WME) followed by centrifugation at 40 g for 3 minutes. Hepatocytes were then resuspended in prewarmed WME at a density of 1.1×10^6 cells/mL and 45 μl of the cell suspension was loaded into a prewarmed 96-well plate and equilibrated for 15 minutes at 37°C. Pretreatment with model compounds were initiated by the addition of 5 μl of prewarmed 10X inhibitor working solution in WME. The final concentration of DMSO in the preincubation was 0.1%. After each preincubation time point, the probe substrate reaction was initiated by addition of 150 μl of prewarmed WME containing the substrate (Table 1). At the end of the incubation time (Table 1), the enzyme reaction was stopped by addition of 50 μl stop solution (0.1% formic acid in acetonitrile containing a stable-isotope labeled internal standard). The plate was stored at -20°C as needed until analysis. The concentrations of probe substrate metabolite formed

TABLE 2

Inhibitors and preincubation conditions

CYP Isoform	Inhibitor	Clinical Inhibition	Concentration Range in Preincubation (μM)	Preincubation Times (min)
CYP1A2	Cimetidine	Weak	16–2000	0, 15, 30, 45, 60
CYP1A2	Ciprofloxacin	Moderate	3.9–500	0, 15, 30, 45, 60
CYP1A2	Fluvoxamine	Strong	0.0046–10	0, 5, 10, 15, 20
CYP2C8	Trimethoprim	Weak	1.5–200	0, 15, 30, 45, 60
CYP2C8	Clopidogrel	Moderate	0.3–600	0, 15, 30, 45, 60
CYP2C8	Gemfibrozil	Strong	0.1–300	0, 15, 30, 45, 60
CYP2C9	Fluvoxamine	Weak	3.1–300	0, 5, 10, 20, 30
CYP2C9	Miconazole	Moderate	1.6–200	0, 5, 10, 20, 30
CYP2C9	Tasisulam	Strong	0.003–10	0, 5, 10, 20, 30
CYP2C19	Omeprazole	Weak	0.03–100	0, 15, 30, 45, 60
CYP2C19	Fluvoxamine	Strong	0.01–30	0, 5, 10, 20, 30
CYP2C19	Fluconazole	Strong	0.03–100	0, 5, 10, 15, 20
CYP2C19	Ticlopidine	Strong	0.01–30	0, 15, 30, 45, 60
CYP2C19	Osilodrostat	Moderate	0.1–300	0, 15, 30, 45, 60
CYP2C19	Moclobemide	Moderate	0.1–300	0, 15, 30, 45, 60
CYP2D6	Dronedarone	Weak	3.1–300	0, 15, 30, 45, 60
CYP2D6	Mirabegron	Moderate	0.0046–10	0, 15, 30, 45, 60
CYP2D6	Paroxetine	Strong	0.0091–20	0, 15, 30, 45, 60

Weak = AUCR ($\geq$1.2- to <2.0-fold), Moderate = AUCR ($\geq$2.0- to <5.0-fold), Strong = AUCR ($\geq$5.0-fold).

TABLE 3

Parameter estimates from pooled human hepatocyte Incubations

CYP Isoform	Inhibitor	Equation	k_{inact} (min-1)	$K_I/K_{I,u}$ (μM)	k_{inact}/K_I (L*min-1*μmol)	95% CI k_{inact} (min-1)		95% CI K_I (μM)	
CYP1A2	Cimetidine	6	0.011	152/142	0.000072	0.0090	0.012	84	271
CYP1A2	Ciprofloxacin	6	0.0066	7.5/7.04	0.00088	0.0050	0.0082	2.9	23
CYP1A2	Fluvoxamine	5	0.35	0.048/0.0356	7.3	Only 2 points used for k_{obs} determinations $K_{i,u}$ = 1.95			
CYP2B6	Ticlopidine[a]	5	0.137	0.489/0.257	0.280	0.12	0.16	0.37	0.66
CYP2C8	Trimethoprim	3	0.011	4.3/3.95	0.0025	0.010	0.012	3.0	6.0
CYP2C8	clopidogrel	3	0.013	3.6/1.53	0.0036	0.010	0.017	0.88	15
CYP2C8	Gemfibrozil	3	0.088	1.5/1.09	0.061	0.080	0.097	0.85	2.4
CYP2C9	Fluvoxamine	6	0.11	32/24.0	0.0034	0.082	0.16	16	71
CYP2C9	Miconazole	3	0.21	15/0.271	0.014	0.19	0.24	10	22
CYP2C9	Tasisulam	6	0.10	2.3/1.05	0.044	0.069	0.17	0.69	8.1
CYP2C19	Omeprazole	3	0.0047	1.0/0.807	0.0048	0.0037	0.0058	0.33	2.6
CYP2C19	Fluvoxamine	6	0.20	5.3/3.94	0.037	0.16	0.25	2.9	9.9
CYP2C19	Fluconazole		No TDI observed			K_i = 22.4 / $K_{i,u}$ = 2.41			
CYP2C19	Osilodrostat		No TDI observed			K_i = 11.3 / $K_{i,u}$ = 1.10			
CYP2C19	Moclobemide				No inhibition observed				
CYP2C19	Ticlopidine[a]	3	0.045	0.52/0.273	0.086	0.038	0.052	0.25	1.0
CYP2D6	Dronedarone	3	0.035	137/9.17	0.00026	0.029	0.045	87.5	226
CYP2D6	Mirabegron	3	0.021	1.3/1.12	0.016	0.015	0.033	0.32	4.8
CYP2D6	Paroxetine	5	0.031	0.61/0.333	0.051	0.026	0.039	0.39	1.0

[a] Ticlopidine parameters were derived using a different pool of hepatocyte donors.

were determined by liquid chromatography tandem mass spectrometry (LC-MS/MS) analysis using previously validated analytical methods (Perloff et al., 2009).

Linearity of metabolite formation with time was confirmed and Michaelis constant (K_m) values determined for all substrates prior to inhibition experiments. Substrate concentrations $\geq$threefold the Michaelis constant (K_m) were chosen for all isoforms. Inhibitors (Table 2) were identified to represent weak, moderate, and strong clinical outcome and incubation concentrations were selected based on available clinical data (reference Supplemental Table 9). Initial preincubation times of 0, 15, 30, 45, and 60 minutes were used for all inhibitors. Follow-up assays using shorter preincubation times were performed when saturation of inactivation resulted in <3 data points available for first order rate constant for inactivation estimated from the slope of residual activity (ln) versus preincubation time at each inhibitor concentration (min^{-1}) (k_{obs}) determination.

Cell viability was assessed by trypan blue exclusion for the highest concentration of inhibitor and vehicle control for the longest preincubation time points. Cell suspension aliquots (25 μl) were sampled and gently mixed with an equal volume of trypan blue (0.4%). Cell number and viability were determined.

Cell viability and observed CYP metabolic activity confirmed a properly functioning hepatocyte model in each assay. Effects of known TDI inhibitors were demonstrated at least once (furafylline (CYP1A2), gemfibrozil (CYP2C8), tienilic acid (CYP2C9), fluvoxamine (CYP2C19), and paroxetine (CYP2D6) but not included in each assay.

TABLE 4

Summary of clinical inhibition data

CYP Isoform	Inhibitor	# of Trials	# of Substrates
1A2	Cimetidine	7	2
	Ciprofloxacin	11	3
	Fluvoxamine	9	6
2C8	Trimethoprim	6	3
	Clopidogrel	6	3
	Gemfibrozil	30	4
2C9	Fluvoxamine	1	1
	Miconazole	1	1
	Tasisulam	1	1
2C19	Omeprazole	4	2
	Osilodrostat	1	1
	Fluconazole	6	3
	Fluvoxamine	16	5
	Ticlopidine	3	1
2D6	Dronedarone	3	1
	Mirabegron	3	3
	Paroxetine	10	6

Human liver microsome incubations. Pooled human liver microsomes supplied by XenoTech (H2610 lot#1710084) were used at a final primary incubation concentration of 1 mg/mL. The primary incubation was equilibrated in a 37°C incubator for 10 minutes followed by the initiation of the reaction by addition of NADPH (final concentration 2 mM). At 0, 5, 10, 20, and 30 minutes preincubation with model inactivator, 7.5 μL aliquots were transferred to a plate containing 142.5 μL saturating concentrations of probe substrate. Reactions were stopped with 300 μL of acetonitrile containing internal standard at 8 minutes for all CYP substrates except paclitaxel (CYP2C8), which was stopped at 12 minutes. Samples were analyzed as previously described (Nishihara et al., 2021).

Positive control inhibitors included furafylline (CYP1A2), gemfibrozil glucuronide (CYP2C8), tienilic acid (CYP2C9), ticlopidine (CYP2C19), and paroxetine (CYP2D6).

LC-MS/MS analysis. Probe substrate metabolites were quantified by LC-MS/MS analysis as described previously (Perloff et al., 2009; Nishihara et al., 2021).

Calculations. For each assay, metabolite concentrations in the incubated samples were quantified using LC-MS/MS analysis by interpolating from the regression line of the standard curves. Standard curves were produced from least squares linear regression analysis of the ratio of metabolite peak area to internal standard peak area versus concentrations of metabolite.

For each concentration of test compound, the raw data from LC-MS/MS quantitation at each time point were normalized to the corresponding solvent control (no inhibitor) to determine % CYP activity remaining as shown in Eq. 1. The normalized data were transformed to natural log (ln) % CYP activity remaining and plotted versus the primary incubation time. The slope was determined from the linear portion of the ln % CYP activity remaining versus primary incubation time curve by linear regression analysis. The negative value of the slope represents k_{obs}, the observed rate constant for inactivation at a specified concentration of inactivator.

$$\text{CYP activity remaining at } [I]_t = C_I/C_{solvent} * 100 \qquad (1)$$

Where C_I is the concentration of metabolite formed in the secondary incubation for each concentration of inhibitor at a primary incubation time point and $C_{solvent}$ is the concentration of metabolite formed in the secondary incubation for the corresponding solvent control primary incubation time point.

An alternate method to determine the k_{obs} was used where % CYP activity remaining at each concentration of inhibitor at each time point was normalized by the CYP activity in the 0 minute vehicle control (Eq. 2). The ln % CYP activity remaining was plotted versus primary incubation time. This method resulted in a k_{obs} value for the solvent control, first order rate

TABLE 5

Enzyme degradation rate

CYP Isoform	K_{deg} (min^{-1})	Reference
CYP1A2	0.00030	(Faber and Fuhr, 2004)
CYP2B6	0.00036	(Renwick et al., 2000)
CYP2C8	0.00053	(Backman et al., 2009)
CYP2C9	0.00011	(Renwick et al., 2000)
CYP2C19	0.00044	
CYP2D6	0.00023	(Liston et al., 2002; Venkatakrishnan and Obach, 2005)

constant for inactivation estimated from the slope of residual activity (ln) versus preincubation time for the solvent control [min^{-1}] (may be constrained to equal the k_{obs} for the vehicle control) ($k_{solvent}$), which is a measure of nonspecific loss of activity during incubation.

$$\% \text{ CYP activity remaining at } [I]_t = C_{I,t\,min}/C_{I,0\,minute\,solvent} * 100 \quad (2)$$

Where $C_{I,t\,min}$ is the concentration of metabolite formed in the secondary incubation at each inhibitor concentration for each time point and $C_{I,0\,minute\,solvent}$ is the concentration of metabolite formed in the secondary incubation in the 0 minute vehicle control.

Non-linear regression models to derive inhibition kinetic parameters. For this study, clinically relevant inactivators of CYPs 1A2, 2C8, 2C9, 2C19, and 2D6 were used to assess suspended hepatocytes as a DDI prediction model. The characteristics of CYP inactivators and the determination of k_{inact} and K_I is extensively described in several papers (Orr et al., 2012; Nagar et al., 2014b; Leow and Chan, 2019) and will be minimally addressed here.

Since the inactivator is considered a substrate of the enzyme being inactivated, the Michaelis-Menten (MM) model was used to determine k_{inact} and K_I as shown in Eq. 3 and an adjusted version of the MM model shown in Eq. 6.

If the k_{obs} was determined using Eq. 1 for % CYP activity remaining, then the MM model described in Eq. 3 was used. If the k_{obs} was determined using Eq. 2 for % CYP activity remaining, then the adjusted MM model described in Eq. 6, which includes an extra parameter, $k_{solvent}$ for the nonspecific loss of activity in the solvent control. The parameters k_{inact} and K_I were then determined by plotting k_{obs} versus [I] and applying nonlinear regression analysis with GraphPad Prism (v. 8, GraphPad Software LLC).

For some experiments nonhyperbolic or atypical MM kinetics such as biphasic and substrate inhibition was observed and Eq. 4 (biphasic) or Eq. 5 (substrate inhibition) models were used. These types of atypical kinetics are considered an artifact of the in vitro system and are discussed in detail

elsewhere (Nagar et al., 2014a). Data points to determine k_{obs} values were chosen using the linear portion of the curves. The best fit models for k_{inact} and K_I determination were chosen using Akaike Information Criterion value and evaluation of the 95% confidence intervals for the parameter estimates.

$$k_{obs} = \frac{k_{inact} \cdot [I]}{K_I + [I]} \quad (3, \text{Michaelis Menten})$$

$$k_{obs} = \frac{k_{inact} \cdot [I] + k_{ratio} \cdot [I] \cdot [I]}{K_I + [I]} \quad (4, \text{Biphasic Kinetics})$$

$$k_{obs} = \frac{k_{inact} \cdot [I]}{K_I + [I] \cdot (1 + \frac{[I]}{K_i})} \frac{k_{inact} \cdot [I]}{K_I + [I] \cdot (1 + \frac{[I]}{K_i})} \quad (5, \text{Substrate Inhibition})$$

$$k_{obs} = k_{solvent} + \frac{k_{inact} \cdot [I]}{K_I + [I]} \quad (6, k\text{solvent correction})$$

Where:

k_{inact} is the maximal inactivation rate constant;

k_{obs} is the observed rate constant for inactivation;

K_I is the concentration of inactivator at which the rate constant of inactivation is half maximal;

$k_{solvent}$ is the observed rate constant for non-specific loss of activity without inhibitor

k_{ratio} is the k_{inact}/inhibition constant for reversible inhibition (K_i) ratio for the second inactivation site that does not reach saturation; and

[I] is the concentration of inactivator in the primary incubation.

For some datasets, the $k_{solvent}$ parameter was added as a constant by adding the absolute value of the slope for the solvent control to the model. This reduced the number of parameters and therefore the degrees of freedom to achieve a better fit.

Evaluation of in vitro to in vivo extrapolation. Basic models in the regulatory guidance documents were used for the initial analysis (Supplementary Table 5). Equation 7 is the equation recommended in the FDA and PMDA DDI guidelines and incorporates a 50-fold correction factor to the unbound $C_{max,ss}$ value. The R_2 equation is presented in Eq. 8 and incorporates the enzyme specific rate of degradation (k_{deg}), (reference Table 5). In addition, the evaluation of IVIVE without the correction factor (Eq. 9) was considered by using alternative correction factors such as 3, 5, 10, and 15.

$$k_{obs} = \frac{k_{inact} \times 50 \times C_{max,u}}{K_{I,u} + 50 \times C_{max,u}} \quad (7)$$

$$R_2 = \frac{k_{obs} + k_{deg}}{k_{deg}} \frac{k_{obs} + k_{deg}}{k_{deg}} \geq 1.25 \quad (8)$$

TABLE 6

Input parameters for the mechanistic static model

Inhibitor	Molecular Weight g/Mol	Log P or D	$F_{u,p}$	F_a	F_g	K_a min^{-1}	R_b	References
Cimetidine	252.34	0.48	0.81	1	0.92	0.012	0.97	(Varma et al., 2010; Burt et al., 2016)
Ciprofloxacin	331.346	0.3	0.60	0.75	0.98	0.01	0.75	(Varma et al., 2010)
Fluvoxamine	318.337	3.0	0.23	1	0.5	0.012	1.5	(Jogiraju et al., 2021)
Trimethoprim	290.321	0.91	0.50	1	0.8	0.0082	1	(Kim et al., 2016)
Clopidogrel	321.826	2.58	0.02	0.5	1	0.08	0.57	(Xu et al., 2020)
Clopidogrel glucuronide	483.92	2.58	0.1	NA	NA	NA	0.57	(Tornio et al., 2014)
Gemfibrozil	250.336	4.3	0.03	1	1	0.1	0.825	(Varma et al., 2015)
Gemfibrozil glucuronide	426.5	3.3	0.115	NA	NA	NA	0.825	
Miconazole	416.134	5.96	0.08	0.1	0.01	0.03	1.5	(O'Reilly et al., 1992; Miki et al., 2011)
Tasisulam	437.09	3.8	0.01	NA	NA	NA	NA	(Perkins et al., 2018)
Omeprazole	345.42	2.43	0.05	1	1	0.1	1	(Marsousi et al., 2018)
Osilodrostat	227.241	2.11	0.636	1	1	0.0467	0.85	(Armani et al., 2017)
Fluconazole	306.275	0.2	0.89	0.98	1	0.0292	1	(Marsousi et al., 2018)
Ticlopidine	263.786	3.6	0.02	1	0.5	0.03	0.55	Default values used
Dronedarone	556.764	5.28	0.01	1	0.898	0.0136	1	(Djebli et al., 2015)
Mirabegron	396.513	2.1	0.27	1	0.68	0.00617	1.42	(Konishi et al., 2019)
Paroxetine	329.369	3.55	0.05	0.93	1	0.017	1.26	(Marsousi et al., 2018)

TABLE 7
Comparison of model fits

Performance	HHEPs				HLM				HHEPs	HLM	HHEPs
	$R_2 \times 3$	Model 1	Model 2	Model 3	R_1	$R_2 \times 3$	Model 1 (Reversible Inhibition Only)	Model 1 (Same Data-Set)	Model 1 (Same Data-Set)	Model 3 (Same Data-Set)	Model 3 (Same Data-Set)
GMFE (90% CI)	9.42 (8.75–10.1)	1.12 (0.89–1.34)	1.16 (0.9–1.4)	0.90 (0.70–1.14)	0.55 (0.22–0.88)	4.02 (3.26–4.78)	0.475 (0.21–0.74)	0.98 (0.67–1.30)	1.0 (0.71–1.35)	0.67 (0.26–1.07)	0.84 (0.46–1.21)
RMSE	284	2.76	3.63	3.67	17.3	5.28	16.5	1.04	0.426	2.71	0.508
% within bioequivalence (0.8–1.25)	2.7	53.8	48.7	45.4	13.9	3.0	15.1	53.0	57.6	48.5	56.1
% within twofold	14.3	91.6	90.8	84.9	52.2	10.6	50.4	87.9	89.4	68.2	74.2
% within threefold	21.4	97.5	97.5	98.3	73.9	34.8	75.6	97.0	95.5	80.3	86.4
# over twofold	96	7	8	3	6	50	1	4	4	2	4
# below twofold	0	3	3	15	49	9	58	4	3	19	13
# of FN	2	0	0	3	13	0	44	0	0	13	3

Model 1 incorporates the reported inhibitor specific parameters to derive the unbound hepatic inlet concentration, whereas Model 1 default inputs K_a = 0.03 min⁻¹ and F_a:F_g = 1, and Model 2 incorporates the $C_{max,ss,u}$ into the equation rather than hepatic inlet concentration.

$$k_{obs} = \frac{k_{inact} \times C_{max,u}}{K_{I,u} \times C_{max,u}} \tag{9}$$

To refine the quantitative prediction, the mechanistic static model (MSM), which enables additive perpetrators, reported elsewhere (Fahmi et al., 2008; Isoherranen et al., 2012) was also used (Eq. 10).

$$\frac{AUC_i}{AUC} = \frac{1}{F_g + (1 - F_g) \times \left(\sum_{k=1}^{n} \frac{fm(E)_{g,k}}{A_{g,k} \times B_{g,k} \times C_{g,k}} + 1 - \sum_{k=1}^{n} fm(E)_{g,k} \right)}$$

$$x \cdot \frac{1}{\sum_{k=1}^{n} \frac{fm\ (E)_{h,k}}{A_{h,k} \times B_{h,k} \times C_{h,k}} + \left(1 - \sum_{k=1}^{n} fm(E)_{h,k} \right)} \tag{10}$$

Where:

A = reversible inhibition, B = time-dependent inhibition, C = induction, g = gut, h = liver and k = enzyme.

Since the enzymes used in this analysis are minimally expressed in enterocytes (Paine et al., 2006; Thelen and Dressman, 2009; Xie et al., 2016), or their expression does not impact DDI outcome (CYP2C9/CYP2C19), (see result section: verification of the lack of importance of CYP2C intestinal expression to DDI) the gut component was removed from Eq. 10. Additionally, since the inhibitors that were evaluated were not inducers, the induction terms were likewise removed, resulting in Eq. 11, which includes Eq. 12, representing the reversible inhibition, and Eq. 13, the time-dependent inhibition in liver.

$$\frac{AUC_i}{AUC} = \frac{1}{\sum_{k=1}^{n} \frac{fm(E)_{h,k}}{A_{h,k} \times B_{h,k}} + \left(1 - \sum_{k=1}^{n} fm(E)_{h,k} \right)} \tag{11}$$

$$A_{h,k} = 1 + \frac{I_{inlet,max,u}}{K_{i,u}} \tag{12}$$

$$B_{h,k} = 1 + \frac{k_{inact} \times I_{inlet,max,u}}{k_{deg,h} \times (I_{inlet,max,u} + K_{I,u})} \tag{13}$$

Calculation of maximal hepatic inlet concentration was conducted using Eq. 14, and the unbound hepatic inlet concentration ($I_{inlet,max,u}$) was calculated with Eq. 15.

$$I_{inlet,max} = Rb \times C_{max,plasma} + \frac{Fa \times Fg \times Ka \times Dose}{Qh} \tag{14}$$

$$I_{inlet,max,u} = \frac{(1 - H) \times f_{u,p}}{Rb} \times I_{inlet,max} \tag{15}$$

Where H is the hematocrit and assumed to be 0.45 and Rb is the blood-to-plasma ratio.

Multiple iterations of the above model with various [I] input values were considered including:

Model 1: Using unbound hepatic inlet concentration as described in regulatory guidance;

Model 2: Using unbound hepatic inlet concentration calculated with default values; and

Model 3: Inputting unbound systemic $C_{max,ss}$ in place of $I_{inlet,max,u}$.

All models were evaluated considering the range of published fraction metabolized through the pathway (Fm) values (Supplemental Table 3), and Model 1 used published Ka, Fa and Fg values where available (Table 6), default values used for Model 2 were Ka (0.03 minute−1), Fa:Fg = 1 and Rb = 0.55. The best universally fitting Fm was selected for the optimized data and is depicted in bold in Supplemental Table 3.

In silico estimation of unbound K_i and K_I values. The Kilford equation (Kilford et al., 2008), Eq. 16, was used to estimate the unbound inhibition parameters. In the case of the experimental conditions employed in these studies, the hepatocyte concentration was 50,000 cells (1 × 10⁶ cells/mL), and there was no additional protein present in the media. An intracellular volume of 6.48 pL was used; the incubation volume was 50 µL, resulting in a V_R of 0.00648 (Note $V_R = V_{cell} \times V_{inc}$). Log P or D values reported in the literature for the inhibitors were used (Table 6).
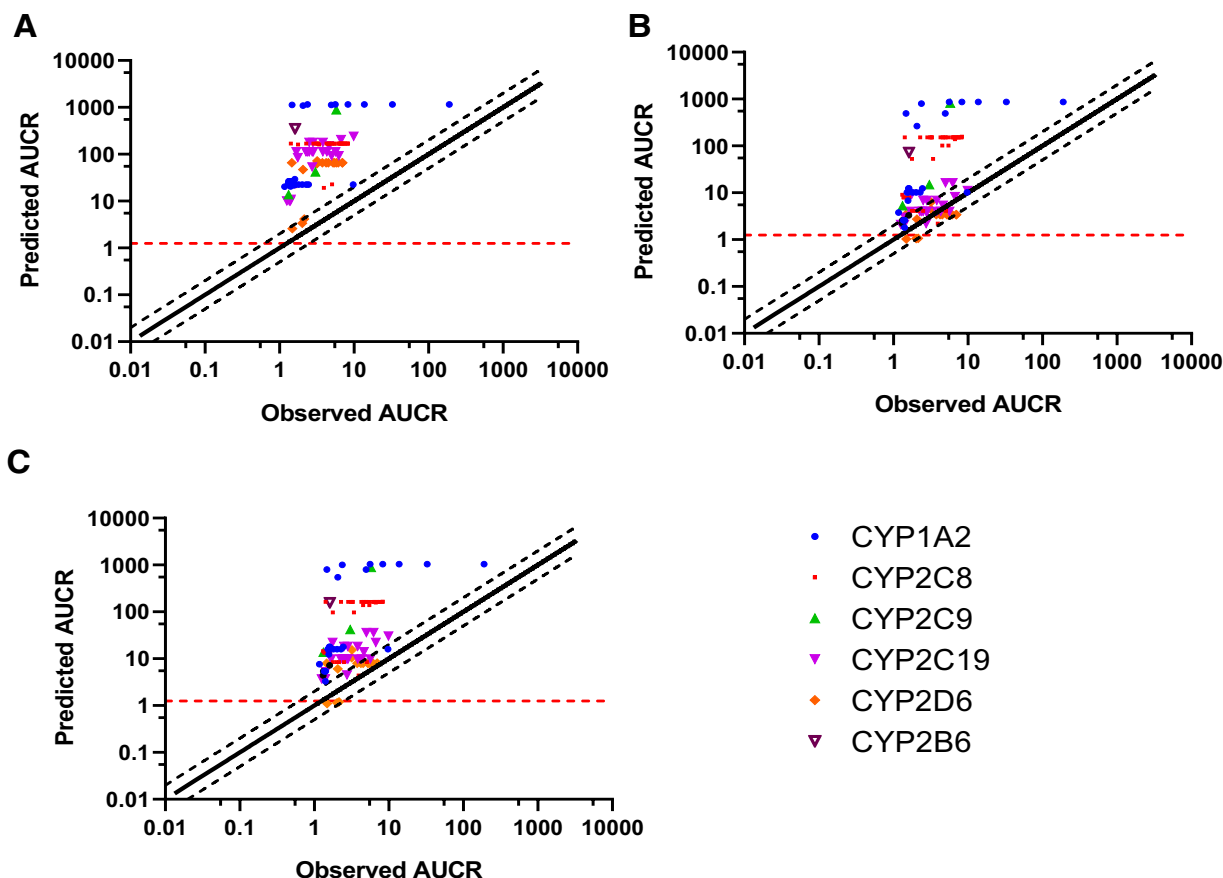
Fig. 2. Predicted AUCR (y-axis) from HHEP data versus observed AUCR (x-axis) for all available clinical data for the selected perpetrators of CYP1A2 (blue circles), CYP2B6 (open purple downward triangle), CYP2C8 (red square), CYP2C9 (green upward triangle), CYP2C19 (purple downward triangle), and CYP2D6 (orange diamond). The solid black line represents the line of unity, and the dashed lines represent twofold margins. The red line shows the cutoff of 1.25 where the calculated R2 value would be considered positive when greater than this cutoff. Panel A depicts the data generated with the recommended inclusion of a 50-fold multiplier to unbound $C_{max,ss}$. Panel B depicts the data with no multiplier and yields one false negative for dronedarone (400, 600, and 800 mg) and CYP2D6. Panel C depicts a threefold multiplier, which reduces false negatives to 0.

$$f_{u,hep} = \frac{1}{1 + 125 \times V_R \times 10^{0.072 \times \log P \ or \ D + 0.067 \times \log P \ or \ D - 1.126}} \quad (16)$$

Correction of in vitro derived IC_{50} values based on saturating substrate concentrations used in the time-dependent inhibition assay was conducted according to Eq. 17 (Cheng and Prusoff, 1973) and assuming competitive inhibition.

$$K_i = \frac{IC_{50}}{1 + \frac{[Substrate]}{K_m}} \quad (17)$$

Statistical analysis of the goodness of fit for IVIVE models evaluated. The accuracy of the prediction of the individual models was evaluated by deriving the geometric mean fold error (GMFE) according to Eq. 18 and the root mean square error (RMSE) according to Eq. 19. GMFE closest to 1 represents the best fit, whereas RMSE approaching 0 does.

$$GMFE = 10^{mean\left(\left|log\frac{predicted\ DDI}{observed\ DDI}\right|\right)} \quad (18)$$

$$RMSE = \sqrt{\frac{\Sigma(predicted\ DDI - observed\ DDI)^2}{number\ of\ predictions}} \quad (19)$$

Results

Selection of Clinically Relevant Inhibitors for In Vitro Data Generation

The search of the UW-DIDB identified weak, moderate, and strong inhibitors toward CYPs 1A2, 2C8, 2C9, 2C19, and 2D6 (Table 2). Although an attempt was made to identify clinically relevant inhibitors

of CYP2B6, studies were limited to no effect or weak inhibition, thus in vitro evaluation was not further pursued and IVIVE was conducted using reported and/or historical values (Supplementary Table 4). Clinical data used for the IVIVE evaluation of selected inhibitors of CYPs 1A2, 2C8, 2C9, 2C19, and 2D6 is presented in Supplementary Table 9.

TDI Results

Time-dependent inhibition was observed for 16 of the 19 evaluated inhibitors, and kinetic parameters could be confidently determined for them using hepatocytes (Table 3). Mild TDI was observed for cimetidine in HLM; however, inactivation parameters could not be confidently estimated. TDI was not observed in HLM, under the experimental conditions, for any other clinically weak inhibitors, but was observed for one moderate and three strong inhibitors. The positive control inhibitors used in the HLM assay demonstrated expected and robust response with kinetic parameters in line with those reported previously. In human hepatocyte incubations, the k_{inact}/K_I ratios trended with the classification from weak to strong clinical inhibition such that the lower the ratio the weaker the observed clinical effect.

Time-dependent inhibition of CYP1A2 in hepatocytes was observed for cimetidine, ciprofloxacin, and fluvoxamine, using phenacetin as the probe substrate. Fluvoxamine showed potent and rapid inhibition of enzyme activity after a 5-minute preincubation but did not show a further decrease in activity with increasing preincubation time. As a result,
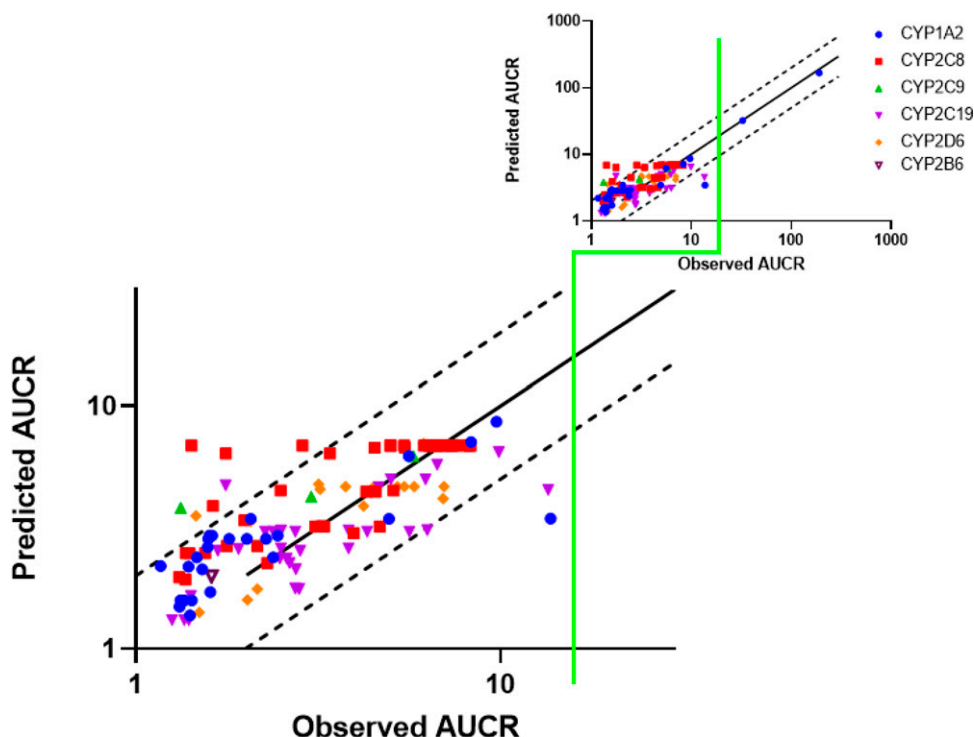
Fig. 3. Predicted AUCR (y-axis) from HHEP data versus observed AUCR (x-axis) for all available clinical data for the selected perpetrators of CYP1A2 (blue circles), CYP2C8 (red square), CYP2C9 (green upward triangle), CYP2C19 (purple downward triangle), CYP2D6 (orange diamond), and CYP2B6 (open purple downward triangle). The solid black line represents the line of unity, and the dashed lines represent twofold margins. The predicted AUCR was generated using the mechanistic static model with the inhibitor specific parameters for F_a, F_g, K_a, and R_b (Table 6) and the F_m value indicated in bold in Supplemental Table 3. The inlet graph expands the axis to include the strong inhibition observed for fluvoxamine against CYP1A2 substrates.

only 2 data points were available to estimate k_{obs} values (Supplemental Fig. 1) resulting in a potential underestimation of inhibitory potency. TDI of CYP1A2 was observed in HLM for only the strong inhibitors, fluvoxamine and furafylline, and not for the weak and moderate inhibitors. The kinetic parameters for fluvoxamine were K_I of 1.81 μM and a K_{inact} of 0.0747 minute^{-1} and for furafylline were K_I of 22.5 μM and a K_{inact} of 0.372 minute^{-1}.

Time-dependent inhibition of CYP2C8 in hepatocytes was observed for trimethoprim, clopidogrel, and gemfibrozil, using amodiaquine as the probe substrate. The inhibition parameters determined from clopidogrel and gemfibrozil were likely due to the glucuronide metabolites as described elsewhere (Ogilvie et al., 2006; Tornio et al., 2014). TDI of CYP2C8 was not observed with the test set in HLM although the positive control, gemfibrozil glucuronide, yielded a total K_I of 29.8 μM and a K_{inact} of 0.04 minute^{-1}.

Time-dependent inhibition of CYP2C9 in hepatocytes was observed for fluvoxamine, miconazole, and tasisulam, using diclofenac as the probe substrate. For fluvoxamine, substantial cytotoxicity was observed at concentrations of 100 μM and above (trypan blue viability of 33% at 200 μM with a 30-minute preincubation). As it is unclear what, if any, impact the decreased viability might have on CYP enzyme activity, the 200 and 300 μM data points were excluded from analysis. TDI of CYP2C9 was not observed with the test set in HLM although the positive control, tienilic acid, yielded a total K_I of 4.35 μM and a K_{inact} of 0.108 minute^{-1}.

Time-dependent inhibition of CYP2C19 was evaluated in human hepatocytes for omeprazole, fluvoxamine, fluconazole, osilodrostat, moclobemide, and ticlopidine. TDI was observed and K_I and k_{inact} values were determined for omeprazole and fluvoxamine. Fluconazole and osilodrostat did not demonstrate TDI, but as both compounds resulted in comparable concentration dependent inhibition at all preincubation

times, K_i values were estimated from the IC$_{50}$ determined at the first time point according to Eq. 17. Moclobemide did not demonstrate any inhibition of CYP2C19 activity in hepatocytes despite resulting in a clinically moderate inhibition of omeprazole clearance [area under the concentration curve ratio (AUCR) = 2.07]. TDI was not observed in HLM for omeprazole, osilodrostat, or fluvoxamine under the incubation conditions used. There was TDI observed for ticlopidine with a total K_I of 85.7 μM and a K_{inact} of 0.111 minute^{-1}.

The inhibition potential for ticlopidine was investigated in this pooled lot of human hepatocytes but did not demonstrate TDI. Of note, historical studies using an alternate set of three donors of hepatocytes have demonstrated time-dependent inhibition of CYP2C19 by ticlopidine and kinetic parameters from those studies were used for the clinical risk assessment. The reason for the difference between donors is unclear. In pooling donors, any impact of polymorphic enzymes should be reduced (Ramsden et al., 2009); however, genotyping data for the donors used in these studies was not available.

Time-dependent inhibition of CYP2D6 was observed for dronedarone in hepatocytes only and for mirabegron and paroxetine in both HLM and human hepatocytes.

Resulting graphs depicting the ln % remaining CYP activity versus incubation time and k_{obs} versus inhibitor concentration are provided in Supplemental Fig. 1.

Verification of the Lack of Importance of CYP2C Intestinal Expression to DDI

It is well recognized that intestinal CYP3A contributes significantly to observed DDI after oral administration of CYP3A perpetrators (Ramsden et al., 2019; Yamada et al., 2020). The impact of intestinal expression of other CYP enzymes is less clear. It is reported that
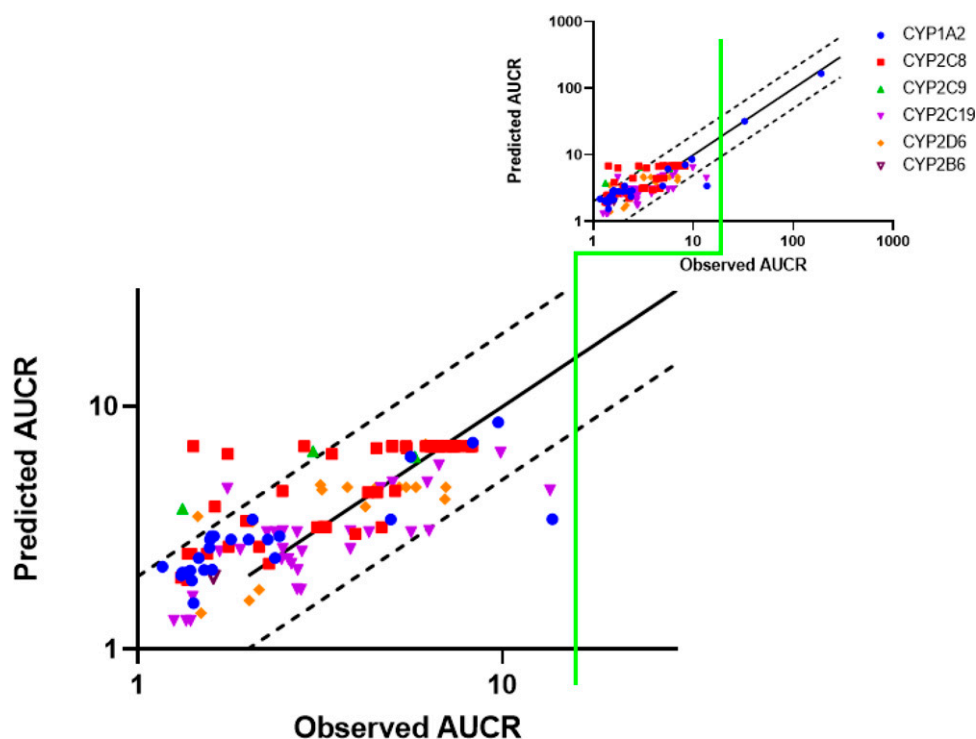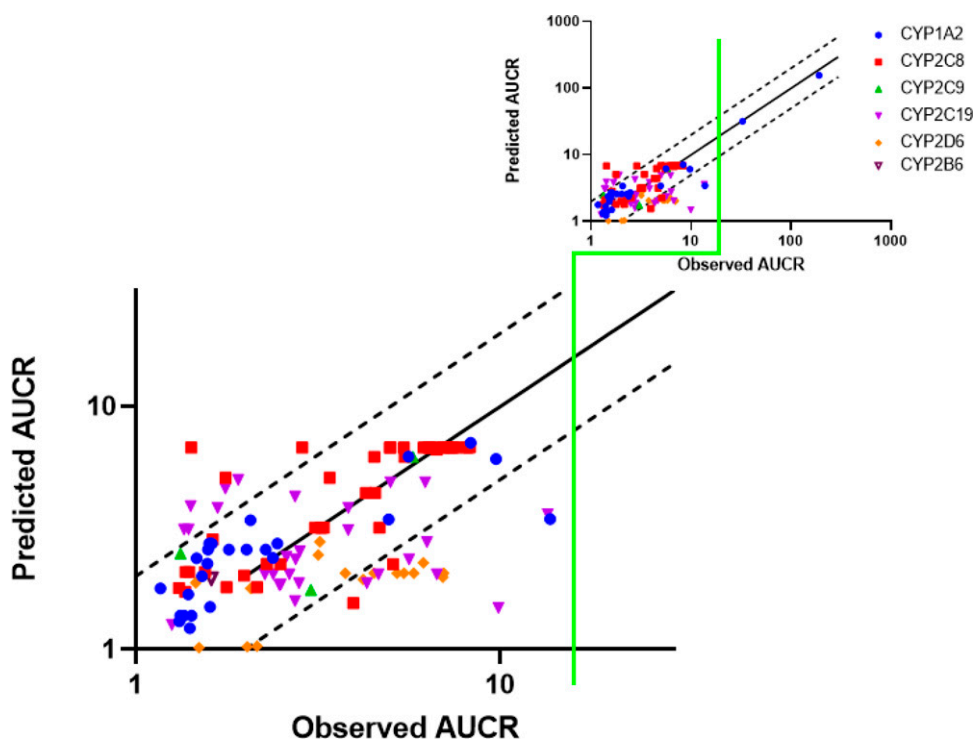
Fig. 4. Predicted AUCR (y-axis) from HHEP data versus observed AUCR (x-axis) for all available clinical data for the selected perpetrators of CYP1A2 (blue circles), CYP2C8 (red square), CYP2C9 (green upward triangle), CYP2C19 (purple downward triangle), CYP2D6 (orange diamond), and CYP2B6 (open purple downward triangle). The solid black line represents the line of unity, and the dashed lines represent twofold margins. The predicted AUCR was generated using the mechanistic static model with the default parameters for F_a (1), F_g (1), K_a (0.03 minute^{-1}), and R_b (0.55) and the F_m value indicated in bold in Supplemental Table 3. The inlet graph expands the axis to include the strong inhibition observed for fluvoxamine against CYP1A2 substrates.

CYP2C9 is the next most abundantly expressed CYP representing 14% of the detected intestinal CYP content, followed by CYP2C19 (2%) and CYP2D6, whereas neither CYP1A2 or CYP2C8 were detected (Paine et al., 2006; Xie et al., 2016). To evaluate the importance of CYP2C9 intestinal expression toward observed DDIs, the clinical inhibition and induction data were reviewed for inhibitors and inducers evaluated against the substrates when dosed IV (hepatic) and orally (hepatic + intestinal) (Supplemental Table 6). As evidenced by the similar magnitudes of change observed when substrates were dosed IV or orally, after administration of the inhibitor or inducer, the impact of intestinal CYP2C9 toward the observed DDI is limited. In addition, the F_g reported for common CYP2C9 substrates including warfarin, tolbutamide, celecoxib, and phenytoin are >0.9, whereby the max percent AUC increase from inhibition at the intestinal level is calculated to be 11%. Since the expression of CYP2C19 and CYP2D6 in the gut is much less than CYP2C9, an assumption is made that the impact of intestinal activity on the magnitude of DDI is also likely to be limited.

How Does the Data Generated in This Study Compare with Literature Values Reported in HLM? Although the scope of the enclosed work did not originally include comparative evaluation of TDI for non-CYP3A enzymes using recombinant CYPs or HLM, conducting these studies in human hepatocytes isn't trivial and evaluation of the predictivity of parameters reported for HLM was performed. To facilitate this analysis, all available in vitro parameters for the selected inhibitors were collated from literature (Supplemental Table 7). In some cases, the inhibitor resulted in time-dependent inhibition of multiple CYPs (cimetidine, dronedarone, fluvoxamine, omeprazole, paroxetine, and ticlopidine). Thus, it is important to understand the selectivity of the clinical probe substrate and whether the potential inhibition of other

CYPs involved in its metabolism needs to be considered in the DDI risk assessment. The available literature data for the inhibitors selected in the analysis conducted herein was limited. Published values were available for gemfibrozil, gemfibrozil glucuronide, omeprazole, osilodrostat, paroxetine, and ticlopidine (for both CYP2B6 and CYP2C19). The inhibition parameters were generated in-house for fluvoxamine, gemfibrozil glucuronide, ticlopidine, mirabegron, and paroxetine. The values were corrected to unbound values using the in silico approach reported by Hallifax and Houston, 2006. In addition, an attempt was made to derive the TDI parameters for the selected test set using the standard protocols established within Takeda. Kinetic parameters could only be derived for a limited number of the inhibitors using HLM under the incubation conditions used. A recent publication highlighted the critical role of passive permeability to differences between clearance and inhibition parameters derived from HHEP and HLM (Keefer et al., 2020). To understand whether the time dependency observed in hepatocytes may be an artifact of low/slow permeability followed by direct inhibition, reported information on the biopharmaceutics classification system and direct inhibition parameters was collected (Supplemental Table 8). These data were used to evaluate the potential for reversible inhibition to recover the observed clinical DDI using the MSM. Using only the reversible inhibition parameters resulted in 44 false negative trials and a large underprediction (58/119 over twofold below the observed magnitude) (Table 7). These results suggest that delayed permeability, followed by direct inhibition, cannot explain the lack of TDI observed in HLM for weak and moderate inhibitors. An additional approach would be to experimentally derive the K_{puu} values in hepatocytes, rather than relying on in silico values. There are a number of proposed methods to derive this value although no consensus has been
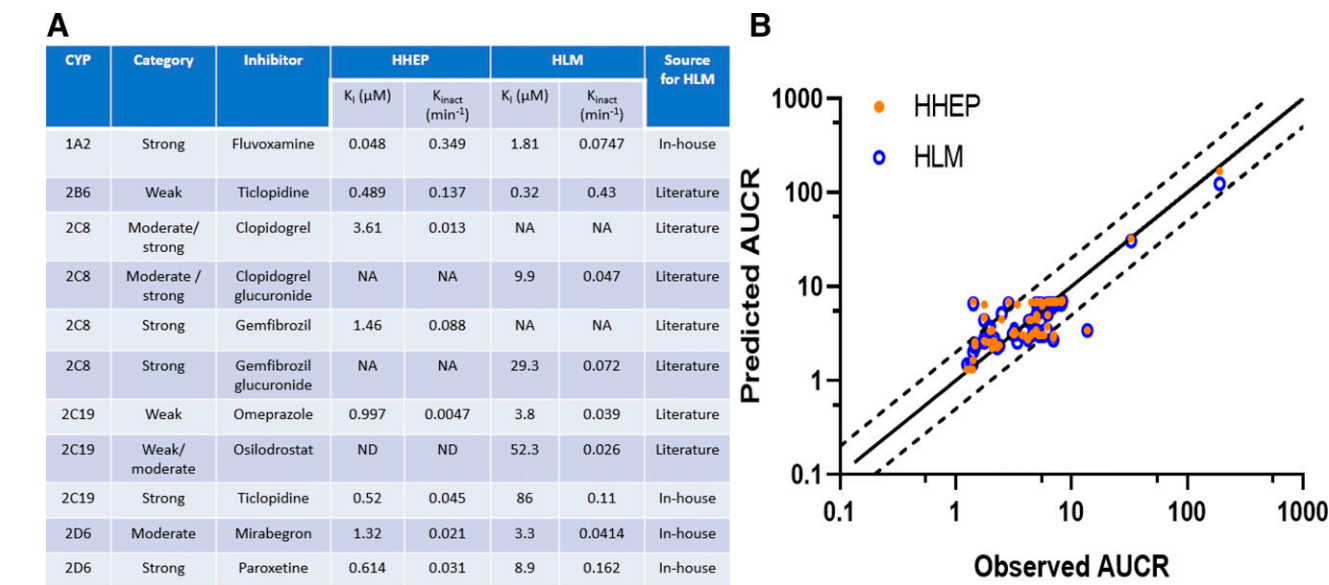
Fig. 5. Predicted AUCR (y-axis) from HHEP data versus observed AUCR (x-axis) for all available clinical data for the selected perpetrators of CYP1A2 (blue circles), CYP2C8 (red square), CYP2C9 (green upward triangle), CYP2C19 (purple downward triangle), CYP2D6 (orange diamond), and CYP2B6 (open purple downward triangle). The solid black line represents the line of unity, and the dashed lines represent twofold margins. The predicted AUCR was generated using the mechanistic static model with the unbound $C_{max,ss}$ and the F_m value indicated in bold in Supplemental Table 3. The inlet graph expands the axis to include the strong inhibition observed for fluvoxamine against CYP1A2 substrates. Of note, this model failed to identify the clinical relevance of dronedarone toward metoprolol, a CYP2D6 substrate.

reached, and therefore K_{puu} values were not determined in the enclosed studies (Chu et al., 2013; Mateus et al., 2013; Riccardi et al., 2016).

Clinical Risk Assessment from In Vitro Inhibition Parameters. The clinical risk assessment was conducted following the recommendations set forth in the regulatory documents (FDA, EMA, and PMDA). The first step was to use the basic models that consider the inhibition kinetic parameters and the maximal unbound plasma concentration at steady state ($C_{max,ss,u}$) but do not incorporate substrate specific parameters (Eq. 7–9). The nominal K_I values were corrected to unbound K_I values using the predicted nonspecific binding to hepatocytes or HLM (Eq. 16). The unbound K_I values were used in the subsequent equations to assess the clinical risk. The degradation rates presented in Table 5 were input into Eq. 8, dependent on the CYP being inhibited. While the inhibitor $C_{max,ss,u}$ values for the enclosed dataset are known, it should be appreciated that this value is often based on a prediction using preclinical data prior to when first-in-human or multiple dose clinical studies have been conducted. The impact of the inhibitor concentration input value should therefore be considered during the clinical risk assessment for new chemical entities. The R_2 value generated with the basic model was compared with the observed AUCR (Supplementary Table 9). The resulting R_2 values using Eq. 8 significantly overpredicted the observed magnitude of DDI (Fig. 2A, Table 7) when K_{obs} were calculated with 50x unbound C_{max} (Eq. 9). When the 50-fold correction factor was removed according to Eq. 7, dronedarone, a weak to moderate inhibitor of CYP2D6, resulted in a false negative at all three clinical dose levels studied (Fig. 2B). The 800 mg dronedarone became a true positive when applying a correction factor of 3 to the R_2 equation; however, both the 400 and 600 mg dose level predictions were considered false negatives (Fig. 2C, Table 7). The next step was to evaluate various iterations of the MSM (Eq. 10). The MSM model incorporates both inhibitor and substrate specific parameters. The F_m value(s) for each

substrate was collected from the literature (Supplemental Table 3). In cases where multiple F_m values were reported, individual and mean values were evaluated in the prediction. In terms of inhibitor specific parameters, the literature was searched for K_a, F_a, F_g, and R_b to support estimation of the hepatic inlet concentration (Table 6) using Eqs. 14 and 15. When the reported values were used to estimate the unbound hepatic inlet concentration and the optimal F_m values for the substrates were used, there were no false negatives and there was good quantitative prediction observed (Fig. 3, Table 7). In this case, 109 of the 119 (92%) clinical studies were predicted within twofold of the observed AUCR and 64 were predicted within bioequivalence or between 0.8- to 1.25-fold of the observed. The magnitude of seven clinical studies was overpredicted (>twofold predicted/observed) and three were underpredicted (<0.5 predicted/observed). Trimethoprim with repaglinide was overpredicted by 2.4-fold. There were three trials with gemfibrozil, which were overpredicted using repaglinide as the probe substrate for CYP2C8 ranging from 2.4- to 4.8-fold; of note, 20 other similarly designed trials fell within twofold of the observed with 15 of them within bioequivalence. A similar observation was made for ticlopidine with omeprazole where one trial was overpredicted by 2.6-fold and the other two trials were predicted within bioequivalence. If the average of the clinical results is used rather than discreet AUC values, these are no longer overpredicted. Similarly, the inhibitors that were underpredicted (fluconazole and fluvoxamine) were well-predicted in all of the other clinical studies, 4/6 and 8/9, respectively. The analysis of these trends is presented in Supplemental Fig. 2. Therefore, it is likely that the variability in outcome observed between clinical interaction studies should be considered in the risk assessment. The importance of substrate selectivity in the magnitude of DDI can be highlighted by the magnitude of inhibition observed for fluvoxamine against CYP1A2 substrates, where the predicted AUCR ranges from 2.38-fold with theophylline to

A

CYP	Category	Inhibitor	HHEP		HLM		Source for HLM
			K_I (µM)	K_{inact} (min^{-1})	K_I (µM)	K_{inact} (min^{-1})	
1A2	Strong	Fluvoxamine	0.048	0.349	1.81	0.0747	In-house
2B6	Weak	Ticlopidine	0.489	0.137	0.32	0.43	Literature
2C8	Moderate/ strong	Clopidogrel	3.61	0.013	NA	NA	Literature
2C8	Moderate / strong	Clopidogrel glucuronide	NA	NA	9.9	0.047	Literature
2C8	Strong	Gemfibrozil	1.46	0.088	NA	NA	Literature
2C8	Strong	Gemfibrozil glucuronide	NA	NA	29.3	0.072	Literature
2C19	Weak	Omeprazole	0.997	0.0047	3.8	0.039	Literature
2C19	Weak/ moderate	Osilodrostat	ND	ND	52.3	0.026	Literature
2C19	Strong	Ticlopidine	0.52	0.045	86	0.11	In-house
2D6	Moderate	Mirabegron	1.32	0.021	3.3	0.0414	In-house
2D6	Strong	Paroxetine	0.614	0.031	8.9	0.162	In-house

B

Fig. 6. Panel A shows the table of the kinetic parameters for the perpetrators with published or in-house derived HLM data. Panel B shows the predicted AUCR (y-axis) versus observed AUCR (x-axis) for all available clinical data for the selected perpetrators with HLM (blue open circles) and HHEP (orange closed circles). Predicted AUCR was derived using the unbound hepatic inlet concentration. The solid black line represents the line of unity, and the dashed lines represent twofold margins.

168-fold with ramelteon. Likewise, the $F_{mCYP1A2}$ for theophylline (0.58) is much lower than that of ramelteon (0.995) as was the magnitude of DDI observed, 1.47- to 2.38-fold for theophylline and 190-fold for ramelteon. Since it is appreciated that the inhibitor specific parameters are often not known during early DDI risk assessment, default values of 1 for F_a:F_g, 0.03 minute^{-1} for K_a and 0.55 for R_b were also evaluated to derive the unbound hepatic inlet concentration. This also resulted in zero false negatives and 108 of 119 (90.8%) trials within twofold and 58 (49%) within bioequivalence. In the case of missed predictions, most (8/11) were overpredicted (Fig. 4). Lastly, the MSM was evaluated using the $C_{max,ss,u}$ rather than the unbound hepatic inlet concentration. Using this inhibitor input value resulted in a higher number of underpredictions (15 < 0.5) and reduced number of values within twofold (84.9%). Clinical risk assessment using the MSM with the $C_{max,ss,u}$ resulted in dronedarone as a false negative (Fig. 5). Using the full dataset available with the HHEPs data and considering the GMFE closest to 1 and the lowest RMSE, Model 1 performed the best followed by Model 2 (default values to derive the hepatic inlet concentration) and lastly Model 3 (Table 7). Since using the $C_{max,ss,u}$ resulted in a significant increase in the number of underpredicted DDI outcome (3 → 15), evaluation of the average unbound systemic plasma concentration at steady state was not conducted. Considering that the available clinical and in vitro parameter dataset for HLM was significantly smaller than HHEPs (66 versus 119) a direct comparison between them was made (Table 7, two far right columns, Fig. 6). In general, the parameters derived from HHEPs performed slightly better than those from HLM when comparing the GMFE and RMSE values. The quantitative accuracy was also higher in HHEPs than HLMs. Consistent with the data observed for the full HHEPs dataset, there were no false negatives (FN) when using the unbound hepatic inlet concentration; whereas there were 3 and 13, for HHEPs and HLM, respectively when inputting the $C_{max,ss,u}$. In the case where $C_{max,ss,u}$ was used as the input parameter, there were 13 false negatives using the HLM data including trials with ticlopidine (3/3), mirabegron (1/3), and paroxetine (9/10) and 3 false negatives using the hepatocyte data (3/4, omeprazole trials), (Table 7). Taken together, these data suggest that

parameters generated from either HLM or HHEPs coupled with the MSM using $I_{inlet,max,u}$ as the input results in quantitative prediction of magnitude of DDI with no false negatives. Since good quantitative predictions were possible using the MSM, which is much easier and more accessible to researchers, Physiologically-Based Pharmacokinetic (PBPK) modeling was not conducted. It is possible that some of the overpredictions might be reduced with PBPK modeling.

Discussion

Clinically relevant TDI has been reported for multiple CYP enzymes, although clinical risk assessments and IVIVE efforts have historically focused on CYP3A as the primary enzyme responsible for the majority of DDI (Obach et al., 2007; Mao et al., 2011; Kenny et al., 2012; Vieira et al., 2014; Tseng et al., 2021). Given the importance of identifying DDI liabilities during drug development, regulatory agencies have proposed guidance on evaluating the DDI potential for NCEs (EMA, FDA, and PMDA). Although clinically relevant TDI has been reported for non-CYP3A enzymes including CYP1A2, CYP2B6, CYP2C8, CYP2C9, CYP2C19, and CYP2D6, to our knowledge a systematic review has not been conducted, and therefore it is unclear whether the proposed recommendations, based on CYP3A data, are appropriate for characterizing the clinical inhibition risk of these non-CYP3A isoforms.

It is appreciated that traditional in vitro studies tend to overpredict the risk for DDI and can be based on a number of assumptions. Similar observations have been reported for competitive inhibition, whereby the inhibitory parameters associated with compounds likely to accumulate within cells due to active uptake were markedly different in experiments conducted using HLM and human hepatocytes (Brown et al., 2010). To this end, experiments were designed using pooled human hepatocytes to derive TDI kinetic parameters with a focus on non-CYP3A enzymes. To investigate the utility of suspended hepatocytes as a tool to better predict TDI, the literature was mined for clinically relevant weak, moderate, and strong inhibitors of CYPs 1A2, 2C8, 2C9, 2C19, and 2D6 using the

UW-DIDB. Inhibitors were selected with clinical inhibition observed under steady state conditions. The literature was further searched to evaluate whether in vitro induction parameters were available for the inhibitor test set, and where these parameters were not available, the assumption was made that the inhibitor was not an inducer. Furthermore, whether the inhibitors were substrates or inhibitors of major drug transporters was also considered. In vitro incubation conditions were established based on validation work conducted by Corning Life Sciences. The in vitro test concentrations used in the evaluation were determined considering the clinical concentrations, solubility, existing data, and toxicity potential with the goal to enable estimation of the in vitro kinetic parameters. The time points were selected to ensure adequate sensitivity for deriving the inhibition rate constants k_{obs}. The in vitro data were fit to various kinetic models to derive the K_I and K_{inact} values, and the model selected was dependent on the shape of the k_{obs} versus concentration profile.

Of the 18 evaluated inhibitors, 16 demonstrated TDI in human hepatocytes, and kinetic parameters could be confidently derived for them. TDI toward CYP2C19 was not observed in hepatocytes for fluconazole or osilodrostat although reversible inhibition parameters could be derived for use in clinical risk assessment with basic models. Fluconazole is known to be a potent reversible inhibitor of CYP2C9, CYP2C19, and CYP3A. As TDI necessitates formation of a reactive metabolite, the lack of TDI by fluconazole is consistent with the knowledge that fluconazole is poorly metabolized and primarily eliminated unchanged via renal excretion (Bellmann and Smuszkiewicz, 2017). The lack of TDI observed for osilodrostat in hepatocytes was in contrast to data generated in HLM, where inactivation parameters could be derived (Armani et al., 2017). However, the DDI observed with omeprazole (AUCR = 1.91) was well predicted using the estimated K_i for reversible inhibition in the mechanistic static model (AUCR = 2.57). Of note, there was no inhibition of CYP2C19 observed for moclobemide in hepatocytes despite a clinically relevant interaction with omeprazole (AUCR = 2.07). Moclobemide has been reported to inhibit CYP2C19 in vitro, and TDI parameters were estimated based on clinical observations of autoinhibition (Kanacher et al., 2020).

Although CYP2B6 inhibitors were not investigated in the current study, due to limited available clinical data, TDI parameters derived in an alternate pool of human hepatocytes, for ticlopidine, were used to conduct clinical risk assessment for clinical data available with CYP2B6 substrates with the goal to evaluate whether the observations made for CYP2B6 were consistent with the other enzymes evaluated. In the enclosed studies, ticlopidine was included as a strong inhibitor toward CYP2C19 since there was clinical data demonstrating AUCR increases up to sixfold for omeprazole. Importantly, ticlopidine did not result in TDI of CYP2C19 in this hepatocyte donor pool; however, TDI kinetic parameters could be derived in the same donor pool as used for CYP2B6, and those were used to evaluate clinical risk predictions and for comparisons with data generated from HLM. It is unclear why there were differences observed between donor pools, although it's important to recognize that this variability exists in the in vitro model. There was limited data available for the selected inhibitors in HLM with only gemfibrozil, gemfibrozil glucuronide, omeprazole, osilodrostat, paroxetine, and ticlopidine having published data. There were no reported inactivation parameters for these inhibitors and enzymes using hepatocytes as the in vitro test system. In general, the available TDI parameters from hepatocytes were limited to CYP3A.

In recent examples, TDI data generated from HLM coupled with PBPK modeling has resulted in quantitative prediction of DDI potential consistent with clinical changes observed (Armani et al., 2017; Perkins et al., 2018; Tseng et al., 2021). While PBPK modeling was in scope for this project, it was not pursued given that quantitative predictions

were observed when applying the MSM. Multiple laboratories have demonstrated improvement in DDI prediction accuracy using human hepatocytes suspended in human plasma particularly for CYP3A inhibitors (Lu et al., 2007; Lu et al., 2008; Mao et al., 2011). Despite the data supporting this observation for CYP3A, data available with non-CYP3A enzymes is lacking, thus plasma was not included in these studies with the aim to limit confounding factors. This is also consistent with the approach taken in a recent study where the authors compared TDI of CYP3A generated for 50 drugs in both HLM and hepatocytes to establish boundary values for k_{obs}, which would reduce the number of false positives observed in their screening assay (Eng et al., 2020). To understand whether the current basic equations recommended in the regulatory guidance documents, which are based on IVIVE for CYP3A, are applicable to TDI for non-CYP3A enzymes, analysis was conducted with the goal of: (1) establishing a multiplier to the "R_2" equation, which would reduce the number of false positives and not result in increased false negatives and (2) establish a quantitative prediction model through investigation of various input parameters in the MSM.

When applying a 50-fold multiplier, as proposed in the R_2 equation within the FDA, and PMDA regulatory guidance, a high rate of overpredictions was observed for data generated in both HHEPs and HLM. When the multiplier is removed, dronedarone became a false positive. It should be noted that dronedarone is highly lipophilic although less so than amiodarone (Hohnloser et al., 2009) which may have led to underestimation of the inactivation parameters from HHEP. When a multiplier of 3 was used, the false negatives were eliminated but the quantitative prediction was still poor (13% within twofold). When the mechanistic static model, which considers the substrate F_m, was used there was good alignment between the predicted DDI and observed DDI even when multiple substrates with varying F_m values were used with the same inhibitor. When the unbound $C_{max,ss}$ concentration was used rather than $I_{inlet,max,u}$, dronedarone was one false negative in HHEPs and there were a significant number of underpredictions (15/18). When the $I_{inlet,max,u}$ was used as the input, along with inhibitor specific values for its derivation (K_a, F_a, F_g, and R_b), there were no false negatives and 92% of the dataset was predicted within twofold of the observed values. Considering that there are situations where these values are unknown, default parameters of 0.03 for K_a, 1 for F_a and F_g and R_b of 0.55, were also evaluated and resulted in 91% of the studies being predicted within twofold. In summary, these studies revealed that quantitative IVIVE for CYP1A2, 2C8, 2C9, 2C19, and 2D6 inhibition is possible when using kinetic parameters generated in HHEPs.

A comparison between HHEPs and HLM was made for nine inhibitors where data were available in literature or generated in-house. It is important to note that of the 17 inhibitors evaluated, using standard HLM conditions, only four exhibited TDI. The reason for this discrepancy is unclear, although it is possible that some optimization of the incubation conditions, such as using a lower protein concentration, may enable TDI detection, as previously published for omeprazole (Ogilvie et al., 2011). Where comparisons were possible, there was a tendency for underprediction of DDI when using the data from HLM compared with HHEPs. This observation is in contrast to recent observations for CYP3A TDI (Tseng et al., 2021). The inactivation parameters generated from HHEP were almost always lower than those generated in HLMs for these non-CYP3A enzymes. This is similar to the observations made for CYP3A, where the authors hypothesized that there may be differences in the enzyme behavior in the intact cell model (Tseng et al., 2021). In that work, the authors further concluded that CYP3A TDI could be accurately predicted using the unbound average hepatic inlet concentration for gut and unbound average circulating concentration for liver, when using the MSM. When TDI inhibitor parameters for non-CYP3A enzymes were coupled with inhibitor and substrate specific

parameters in the MSM, there were a number of FN and underpredictions observed when using the $C_{max,ss,u}$, and therefore evaluation of $C_{avg,ss,u}$ was not pursued. A notable difference between the assessment for CYP3A and non-CYP3A DDI is the importance of gut CYP3A in the overall magnitude of the observed DDI. Presumably the concentration used to project hepatic DDI would be consistent across CYP enzymes, suggesting that further optimization of the gut input is warranted for predicting CYP3A inhibition DDI.

Results from this study show that incorporating kinetic parameters for TDI into the previously proposed MSM enables quantitative prediction of TDI for CYPs 1A2, 2B6, 2C8, 2C9, 2C19, and 2D6. Additionally, analysis of the available HLM data also demonstrates reasonable quantitative prediction using the MSM, confirming that in vitro parameters derived from HLM are likewise valuable for TDI risk assessment from non-CYP3A enzymes, although the analysis would benefit from additional data points.

Authorship Contributions

Participated in research design: Ramsden, Perloff, Whitcher-Johnstone, Zhang.

Conducted experiments: Ho, Patel, Kozminski, Fullenwider.

Performed data analysis: Ramsden, Perloff, Whitcher-Johnstone, Kozminski, Fullenwider.

Wrote or contributed to the writing of the manuscript: Ramsden, Perloff, Whitcher-Johnstone, Zhang.

References

Armani S, Ting L, Sauter N, Darstein C, Tripathi AP, Wang L, Zhu B, Gu H, Chun DY, Einolf HJ, et al. (2017) Drug interaction potential of osilodrostat (LCI699) based on its effect on the pharmacokinetics of probe drugs of cytochrome P450 enzymes in healthy adults. *Clin Drug Investig* 37:465–472.

Backman JT, Honkalammi J, Neuvonen M, Kurkinen KJ, Tornio A, Niemi M, and Neuvonen PJ (2009) CYP2C8 activity recovers within 96 hours after gemfibrozil dosing: estimation of CYP2C8 half-life using repaglinide as an in vivo probe. *Drug Metab Dispos* 37:2359–2366.

Bellmann R and Smuszkiewicz P (2017) Pharmacokinetics of antifungal drugs: practical implications for optimized treatment of patients. *Infection* 45:737–779.

Brown HS, Wilby AJ, Alder J, and Houston JB (2010) Comparative use of isolated hepatocytes and hepatic microsomes for cytochrome P450 inhibition studies: transporter-enzyme interplay. *Drug Metab Dispos* 38:2139–2146.

Burt HJ, Neuhoff S, Almond L, Gaohua L, Harwood MD, Jamei M, Rostami-Hodjegan A, Tucker GT, and Rowland-Yeo K (2016) Metformin and cimetidine: physiologically based pharmacokinetic modelling to investigate transporter mediated drug-drug interactions. *Eur J Pharm Sci* 88:70–82.

Chen Y, Liu L, Monshouwer M, and Fretland AJ (2011) Determination of time-dependent inactivation of CYP3A4 in cryopreserved human hepatocytes and assessment of human drug-drug interactions. *Drug Metab Dispos* 39:2085–2092.

Chu X, Korzekwa K, Elsby R, Fenner K, Galetin A, Lai Y, Matsson P, Moss A, Nagar S, Rosania GR, et al.; International Transporter Consortium (2013) Intracellular drug concentrations and transporters: measurement, modeling, and implications for the liver. *Clin Pharmacol Ther* 94:126–141.

Djebli N, Fabre D, Boulenc X, Fabre G, Sultan E, and Hurbin F (2015) Physiologically based pharmacokinetic modeling for sequential metabolism: effect of CYP2C19 genetic polymorphism on clopidogrel and clopidogrel active metabolite pharmacokinetics. *Drug Metab Dispos* 43:510–522.

Eng H, Tseng E, Cerny MA, Goosen TC, and Obach RS (2020) Cytochrome P450 3A time-dependent inhibition assays are too sensitive for identification of drugs causing clinically significant drug-drug interactions: a comparison of human liver microsomes and hepatocytes and definition of boundaries for inactivation rate constants. *Drug Metab Dispos* 49:442–450.

Faber MS and Fuhr U (2004) Time response of cytochrome P450 1A2 activity on cessation of heavy smoking. *Clin Pharmacol Ther* 76:178–184.

Fahmi OA, Maurer TS, Kish M, Cardenas E, Boldt S, and Nettleton D (2008) A combined model for predicting CYP3A4 clinical net drug-drug interaction based on CYP3A4 inhibition, inactivation, and induction determined in vitro. *Drug Metab Dispos* 36:1698–1708.

Grimm SW, Einolf HJ, Hall SD, He K, Lim HK, Ling KH, Lu C, Nomeir AA, Seibert E, Skordos KW, et al. (2009) The conduct of in vitro studies to address time-dependent inhibition of drug-

metabolizing enzymes: a perspective of the pharmaceutical research and manufacturers of America. *Drug Metab Dispos* 37:1355–1370.

Hallifax D and Houston JB (2006) Binding of drugs to hepatic microsomes: comment and assessment of current prediction methodology with recommendation for improvement. *Drug Metab Dispos* 34:724–726, author reply 727.

Hohnloser SH, Crijns HJ, van Eickels M, Gaudin C, Page RL, Torp-Pedersen C, Connolly SJ; ATHENA Investigators (2009) Effect of dronedarone on cardiovascular events in atrial fibrillation. *N Engl J Med* 360:668–678.

Isoherranen N, Lutz JD, Chung SP, Hachad H, Levy RH, and Ragueneau-Majlessi I (2012) Importance of multi-p450 inhibition in drug-drug interactions: evaluation of incidence, inhibition magnitude, and prediction from in vitro data. *Chem Res Toxicol* 25:2285–2300.

Jogiraju VK, Heimbach T, Toderika Y, and Taft DR (2021) Physiologically based pharmacokinetic modeling of altered tizanidine systemic exposure by CYP1A2 modulation: impact of drug-drug interactions and cigarette consumption. *Drug Metab Pharmacokinet* 37:100375.

Kanacher T, Lindauer A, Mezzalana E, Michon I, Veau C, Mantilla JDG, Nock V, and Fleury A (2020) A physiologically-based pharmacokinetic (PBPK) model network for the prediction of CYP1A2 and CYP2C19 drug-drug-gene interactions with fluvoxamine, omeprazole, S-mephenytoin, moclobemide, tizanidine, mexiletine, ethinylestradiol, and caffeine. *Pharmaceutics* 12:1191.

Keefer C, Chang G, Carlo A, Novak JJ, Banker M, Carey J, Cianfrogna J, Eng H, Jagla C, Johnson N, et al. (2020) Mechanistic insights on clearance and inhibition discordance between liver microsomes and hepatocytes when clearance in liver microsomes is higher than in hepatocytes. *Eur J Pharm Sci* 155:105541.

Kenny JR, Mukadam S, Zhang C, Tay S, Collins C, Galetin A, and Khojasteh SC (2012) Drug-drug interaction potential of marketed oncology drugs: in vitro assessment of time-dependent cytochrome P450 inhibition, reactive metabolite formation and drug-drug interaction prediction. *Pharm Res* 29:1960–1976.

Kilford PJ, Gertz M, Houston JB, and Galetin A (2008) Hepatocellular binding of drugs: correction for unbound fraction in hepatocyte incubations using microsomal binding or drug lipophilicity data. *Drug Metab Dispos* 36:1194–1197.

Kim SJ, Yoshikado T, Ieiri I, Maeda K, Kimura M, Irie S, Kusuhara H, and Sugiyama Y (2016) Clarification of the mechanism of clopidogrel-mediated drug-drug interaction in a clinical cassette small-dose study and its prediction based on in vitro information. *Drug Metab Dispos* 44:1622–1632.

Konishi K, Minematsu T, Nagasaka Y, and Tabata K (2019) Physiologically-based pharmacokinetic modeling for mirabegron: a multi-elimination pathway mediated by cytochrome P450 3A4, uridine 5'-diphosphate-glucuronosyltransferase 2B7, and butyrylcholinesterase. *Xenobiotica* 49:912–921.

Kostrubsky VE, Strom SC, Hanson J, Urda E, Rose K, Burliegh J, Zocharski P, Cai H, Sinclair JF, and Sahi J (2003) Evaluation of hepatotoxic potential of drugs by inhibition of bile-acid transport in cultured primary human hepatocytes and intact rats. *Toxicol Sci* 76:220–228.

Kurnik D, Wood AJ, and Wilkinson GR (2006) The erythromycin breath test reflects P-glycoprotein function independently of cytochrome P450 3A activity. *Clin Pharmacol Ther* 80:228–234.

Lam JL, Okochi H, Huang Y, and Benet LZ (2006) In vitro and in vivo correlation of hepatic transporter effects on erythromycin metabolism: characterizing the importance of transporter-enzyme interplay. *Drug Metab Dispos* 34:1336–1344.

Leow JWH and Chan ECY (2019) Atypical Michaelis-Menten kinetics in cytochrome P450 enzymes: a focus on substrate inhibition. *Biochem Pharmacol* 169:113615.

Liston HL, DeVane CL, Boulton DW, Risch SC, Markowitz JS, and Goldman J (2002) Differential time course of cytochrome P450 2D6 enzyme inhibition by fluoxetine, sertraline, and paroxetine in healthy volunteers. *J Clin Psychopharmacol* 22:169–173.

Lu C, Hatsis P, Berg C, Lee FW, and Balani SK (2008) Prediction of pharmacokinetic drug-drug interactions using human hepatocyte suspension in plasma and cytochrome P450 phenotypic data. II. In vitro-in vivo correlation with ketoconazole. *Drug Metab Dispos* 36:1255–1260.

Lu C, Miwa GT, Prakash SR, Gan LS, and Balani SK (2007) A novel model for the prediction of drug-drug interactions in humans based on in vitro cytochrome p450 phenotypic data. *Drug Metab Dispos* 35:79–85.

Mao J, Mohutsky MA, Harrelson JP, Wrighton SA, and Hall SD (2011) Prediction of CYP3A-mediated drug-drug interactions using human hepatocytes suspended in human plasma. *Drug Metab Dispos* 39:591–602.

Marsousi N, Desmeules JA, Rudaz S, and Daali Y (2018) Prediction of drug-drug interactions using physiologically-based pharmacokinetic models of CYP450 modulators included in Simcyp software. *Biopharm Drug Dispos* 39:3–17.

Mateus A, Matsson P, and Artursson P (2013) Rapid measurement of intracellular unbound drug concentrations. *Mol Pharm* 10:2467–2478.

Miki A, Ohtani H, and Sawada Y (2011) Warfarin and miconazole oral gel interactions: analysis and therapy recommendations based on clinical data and a pharmacokinetic model. *J Clin Pharm Ther* 36:642–650.

Nagar S, Argikar UA, and Tweedie DJ (2014a) Enzyme kinetics in drug metabolism: fundamentals and applications. *Methods Mol Biol* 1113:1–6.

Nagar S, Jones JP, and Korzekwa K (2014b) A numerical method for analysis of in vitro time-dependent inhibition data. Part 1. Theoretical considerations. *Drug Metab Dispos* 42:1575–1586.

Nishihara M, Ramsden D, and Balani SK (2021) Evaluation of the drug-drug interaction potential for trazpiroben (TAK-906), a D₂/D₃ receptor antagonist for gastroparesis, towards cytochrome P450s and transporters. *Xenobiotica* 51:668–679.

O'Reilly RA, Goulart DA, Kunze KL, Neal J, Gibaldi M, Eddy AC, and Trager WF (1992) Mechanisms of the stereoselective interaction between miconazole and racemic warfarin in human subjects. *Clin Pharmacol Ther* 51:656–667.

Obach RS, Walsky RL, and Venkatakrishnan K (2007) Mechanism-based inactivation of human cytochrome p450 enzymes and the prediction of drug-drug interactions. *Drug Metab Dispos* 35:246–255.

Ogilvie BW, Yerino P, Kazmi F, Buckley DB, Rostami-Hodjegan A, Paris BL, Toren P, and Parkinson A (2011) The proton pump inhibitor, omeprazole, but not lansoprazole or pantoprazole, is a metabolism-dependent inhibitor of CYP2C19: implications for coadministration with clopidogrel. *Drug Metab Dispos* 39:2020–2033.

Ogilvie BW, Zhang D, Li W, Rodrigues AD, Gipson AE, Holsapple J, Toren P, and Parkinson A (2006) Glucuronidation converts gemfibrozil to a potent, metabolism-dependent inhibitor of CYP2C8: implications for drug-drug interactions. *Drug Metab Dispos* 34:191–197.

Orr ST, Ripp SL, Ballard TE, Henderson JL, Scott DO, Obach RS, Sun H, and Kalgutkar AS (2012) Mechanism-based inactivation (MBI) of cytochrome P450 enzymes: structure-activity relationships and discovery strategies to mitigate drug-drug interaction risks. *J Med Chem* 55:4896–4933.

Paine MF, Hart HL, Ludington SS, Haining RL, Rettie AE, and Zeldin DC (2006) The human intestinal cytochrome P450 "pie". *Drug Metab Dispos* 34:880–886.

Parkinson A, Kazmi F, Buckley DB, Yerino P, Ogilvie BW, and Paris BL (2010) System-dependent outcomes during the evaluation of drug candidates as inhibitors of cytochrome P450 (CYP) and uridine diphosphate glucuronosyltransferase (UGT) enzymes: human hepatocytes versus liver microsomes versus recombinant enzymes. *Drug Metab Pharmacokinet* **25**:16–27.

Perkins EJ, Posada M, Kellie Turner P, Chappell J, Ng WT, and Twelves C (2018) Physiologically based pharmacokinetic modelling of cytochrome P450 2C9-related tolbutamide drug interactions with sulfaphenazole and tasisulam. *Eur J Drug Metab Pharmacokinet* **43**:355–367.

Perloff ES, Mason AK, Dehal SS, Blanchard AP, Morgan L, Ho T, Dandeneau A, Crocker RM, Chandler CM, Boily N, et al. (2009) Validation of cytochrome P450 time-dependent inhibition assays: a two-time point IC50 shift approach facilitates kinact assay design. *Xenobiotica* **39**:99–112.

Ramsden D, Fung C, Hariparsad N, Kenny JR, Mohutsky M, Parrott NJ, Robertson S, and Tweedie DJ (2019) Perspectives from the Innovation and Quality Consortium Induction Working Group on factors impacting clinical drug-drug interactions resulting from induction: focus on cytochrome 3A substrates. *Drug Metab Dispos* **47**:1206–1221.

Ramsden D, Wallace G, Smith C, and Chan T (2009) A distribution analysis of cytochrome P450 Enzyme activities in cryopreserved human hepatocytes from over 400 individuals. *ISSX* **225**.

Renwick AB, Watts PS, Edwards RJ, Barton PT, Guyonnet I, Price RJ, Tredger JM, Pelkonen O, Boobis AR, and Lake BG (2000) Differential maintenance of cytochrome P450 enzymes in cultured precision-cut human liver slices. *Drug Metab Dispos* **28**:1202–1209.

Riccardi K, Li Z, Brown JA, Gorgoglione MF, Niosi M, Gosset J, Huard K, Erion DM, and Di L (2016) Determination of unbound partition coefficient and in vitro-in vivo extrapolation for SLC13A transporter-mediated uptake. *Drug Metab Dispos* **44**:1633–1642.

Seelig A and Landwojtowicz E (2000) Structure-activity relationship of P-glycoprotein substrates and modifiers. *Eur J Pharm Sci* **12**:31–40.

Thelen K and Dressman JB (2009) Cytochrome P450-mediated metabolism in the human gut wall. *J Pharm Pharmacol* **61**:541–558.

Tornio A, Filppula AM, Kailari O, Neuvonen M, Nyrönen TH, Tapaninen T, Neuvonen PJ, Niemi M, and Backman JT (2014) Glucuronidation converts clopidogrel to a strong time-dependent inhibitor of CYP2C8: a phase II metabolite as a perpetrator of drug-drug interactions. *Clin Pharmacol Ther* **96**:498–507.

Tseng E, Eng H, Lin J, Cerny MA, Tess DA, Goosen TC, and Obach RS (2021). Static and dynamic projections of drug-drug interactions caused by cytochrome P450 3A time-dependent inhibitors measured in human liver microsomes and hepatocytes. *Drug Metab Dispos* **49**:947–960.

Varma MV, Lin J, Bi YA, Kimoto E, and Rodrigues AD (2015) Quantitative rationalization of gemfibrozil drug interactions: consideration of transporters-enzyme interplay and the role of circulating metabolite gemfibrozil 1-O-β-glucuronide. *Drug Metab Dispos* **43**:1108–1118.

Varma MV, Obach RS, Rotter C, Miller HR, Chang G, Steyn SJ, El-Kattan A, and Troutman MD (2010) Physicochemical space for optimum oral bioavailability: contribution of human intestinal absorption and first-pass elimination. *J Med Chem* **53**:1098–1108.

Venkatakrishnan K and Obach RS (2005) In vitro-in vivo extrapolation of CYP2D6 inactivation by paroxetine: prediction of nonstationary pharmacokinetics and drug interaction magnitude. *Drug Metab Dispos* **33**:845–852.

Vieira ML, Kirby B, Ragueneau-Majlessi I, Galetin A, Chien JY, Einolf HJ, Fahmi OA, Fischer V, Fretland A, Grime K, et al. (2014) Evaluation of various static in vitro-in vivo extrapolation models for risk assessment of the CYP3A inhibition potential of an investigational drug. *Clin Pharmacol Ther* **95**:189–198.

Xie F, Ding X, and Zhang QY (2016) An update on the role of intestinal cytochrome P450 enzymes in drug disposition. *Acta Pharm Sin B* **6**:374–383.

Xu L, Chen Y, Pan Y, Skiles GL, and Shou M (2009) Prediction of human drug-drug interactions from time-dependent inactivation of CYP3A4 in primary hepatocytes using a population-based simulator. *Drug Metab Dispos* **37**:2330–2339.

Xu RJ, Kong WM, An XF, Zou JJ, Liu L, and Liu XD (2020) Physiologically-based pharmacokinetic-pharmacodynamics model characterizing CYP2C19 polymorphisms to predict clopidogrel pharmacokinetics and its anti-platelet aggregation effect following oral administration to coronary artery disease patients with or without diabetes. *Front Pharmacol* **11**:593982.

Yamada M, Inoue SI, Sugiyama D, Nishiya Y, Ishizuka T, Watanabe A, Watanabe K, Yamashita S, and Watanabe N (2020) Critical impact of drug-drug interactions via intestinal CYP3A in the risk assessment of weak perpetrators using physiologically based pharmacokinetic models. *Drug Metab Dispos* **48**:288–296.

Zetterberg C, Maltais F, Laitinen L, Liao S, Tsao H, Chakilam A, and Hariparsad N (2016) VX-509 (decernotinib)-mediated CYP3A time-dependent inhibition: an aldehyde oxidase metabolite as a perpetrator of drug-drug interactions. *Drug Metab Dispos* **44**:1286–1295.x

Address correspondence to: Diane Ramsden, 35 Gatehouse Park, Waltham, MA 02451. E-mail: diane.ramsden@takeda.com; or Elke S. Perloff, 6 Henshaw Street, Woburn, MA 01801. E-mail: perloffe@corning.com